Journal of the European Ceramic Society 19 (1999) 601–608

PII: S0955-2219(98)00230-1
0955-2219/99/$—see front matter

In-Situ Determination of Bridging Stresses in Al_2O_3/Al_2O_3-platelet Composites by Fluorescence Spectroscopy

Giuseppe Pezzotti,[a]* Hajime Okuda,[a] Naoki Muraki[b] and Toshihiko Nishida[a]

[a]Department of Materials, Kyoto Institute of Technology, Sakyo-ku, Matsugasaki, 606-8585 Kyoto, Japan
[b]Materials Science Laboratory, Toray Research Center, Inc., Sonoyama, 520 Shiga, Japan

(Received 16 July 1998; accepted 20 September 1998)

Abstract

Bridging stresses arising from interlocking and frictional effects in the crack wake have been quantitatively evaluated in an Al_2O_3/Al_2O_3-platelet ceramic, using in-situ *microprobe fluorescence spectroscopy. Crack opening displacement (COD) profile has also been quantitatively measured in the scanning electron microscope (SEM), in order to substantiate the reliability of the piezo-spectroscopic measurements of microscopic bridging stresses. Mapping the crack wake (at critical condition for crack propagation) with a laser probe of 2 μm spatial resolution led to determine a discrete map of closure stresses over a crack extension of about 800 μm. Relatively high bridging stress values ≈350 MPa were revealed due to platelet interlocking in a near-tip bridging zone <100 μm, whereas frictional sites of lower stress magnitude <100 MPa were monitored in the crack profile farther away from the crack tip. The availability of microscopic fracture parameters like as the bridging stress distribution and the near-tip COD profile enables to quantitatively explain the rising* R-*curve behavior of the Al_2O_3/Al_2O_3-platelet material. Bridging stress distribution, COD profile and* R-*curve data are discussed in comparison with those collected in previous studies on equiaxed Al_2O_3 and toughened Si_3N_4. The present study supports the notion that crack bridging is by far the most important toughening mechanism in non-transforming ceramics.* © *1999 Elsevier Science Limited. All rights reserved*

Keywords: Al_2O_3, platelets, composites, bridging stresses, spectroscopy.

*To whom correspondence should be addressed. Fax: +81-75-724-7580; e-mail: pezzotti@chem.kit.ac.jp

1 Introduction

Our recent contribution to the field of ceramic toughening has been to directly measure the magnitude of crack bridging tractions using microprobe fluorescence or Raman spectroscopy.[1–5] In these measurements, fracture experiments are performed *in situ* into a Raman apparatus and, upon the application of an external load on a precracked specimen, the microscopic tensile stresses developed in the bridging crystallises are collected by focussing a sharp laser beam on each individual bridging site. Stresses are revealed from the shift of the fluorescence or Raman bands, according to a calibration which has to be preliminary performed for each particular ceramic investigated.

In both the elastic[6] and the frictional[7] bridging mechanisms, the toughening effect is expected to be more pronounced in ceramic microstructures with elongated grain morphology. For example, acicular grains in polycrystalline Si_3N_4 were found to elastically bridge the propagating crack and tensile stresses of GPa order were measured *in situ* in these bridging grains by Raman micro-probe spectroscopy.[2] An important characteristic of the bridging stress distribution observed in Si_3N_4 was that the characteristic zone over which elastic bridging develops, was limited to an extension of only ≈100 μm behind the crack tip. The remarkable magnitude of the elastic bridging tractions and their very near-tip character originates the sharply rising *R*-curve behavior observed in Si_3N_4 ceramic. On the other hand, a fluorescence microprobe spectroscopy analysis similarly performed in a large-grained polycrystalline Al_2O_3 with an equiaxed microstructure revealed no elastic bridging effect.[1] A distribution of bridging stresses of low magnitude (i.e. <50 MPa) was detected. These

stresses were due to grain interlocking and friction. Despite their low magnitude, the frictional stresses of Al_2O_3 could develop over a millimeter-size bridging zone and, given the cumulative character of toughening by crack bridging, they led to some tangible rising *R*-curve effect upon a millimeter sized crack extension.

In this paper, the bridging stress distribution is examined by *in-situ* fluorescence spectroscopy in a polycrystalline Al_2O_3 with a plate-like grain microstructure. A fraction of Al_2O_3 platelets is homogeneously dispersed in the equiaxed Al_2O_3-grain structure to promote the bridging effect and, thus, to enhance the rising *R*-curve behavior of the material. The primary goal of the present experiments is to compare the bridging stress distribution developed during fracture in the platelet-toughened Al_2O_3 with those found in equiaxed Al_2O_3 and toughened Si_3N_4 materials, according to previous studies.[12] A confirmation of the bridging stress data obtained by microprobe spectroscopy is also attempted by monitoring the COD profile into the SEM, according to a technique previously established by Rödel *et al.*[8] Then, a theoretical discussion is given, which attempts to relate the microscopic bridging stress distribution and the experimental near-tip COD profile to the macroscopic rising *R*-curve, behavior.

2 Experimental Procedure

High-purity Al_2O_3 powder (AKP-53, Sumitomo Chemical Ltd.) was added with 25 vol% Al_2O_3 platelets (Lonza, Co.; average size: 10 μm, average aspect ratio: 3.5) and mixed by ball milling in ethanol for 1 h. After cold-isostatically preforming, hot pressing was performed in argon at 1500 °C under 30 MPa. The holding time at the maximum temperature was 1 h. The relative density of the material after hot pressing was $\approx$98·5%. In comparison, two model materials, which were examined in previous studies[1,2] are also considered. They are: (*i*) a monolitic Al_2O_3 with equiaxed grain structure, whose average grain size is $\approx$20 μm; and, (*ii*) a Si_3N_4 material toughened by *in-situ* grown acicular grains (average grain diameter and length $\approx$6 and 95 μm, respectively). The processing details regarding these two materials are given elsewhere.[1,2]

Specimens for fracture mechanics testing were cut as parallelepipeds 3×4×20 mm, in dimensions. A straight-through notch of about 1·5 mm depth was first introduced in the center of the bars using a diamond cutter of blade thickness of 0·2 mm. Then, the bottom part of the saw-notch was sharpened using a sharp razor blade sprinkled with fine diamond paste to a radius of $< 10\,\mu$m.[9] Stable crack propagation in bending geometry was obtained using the crack stabilizer designed by Nojima and Nakai[10] for the three-point bending configuration. The span of the loading jig was 16 mm. The details of the crack stabilizer apparatus are given elsewhere.[10,11] *R*-curve data were collected from stable load-displacement curves at a cross-head speed of 0·1 mm min^{-1}. The crack length was measured by traveling optical microscopy during crack propagation. On the other hand, measurements of COD profiles, which require submicrometer resolution, were performed using a field-emission (FE) SEM apparatus (Hitachi, S-800). Fracture mechanics specimens containing stably propagated cracks were re-loaded in a three-point bending jig (span 16 mm) by a manual micrometer device equipped with a load cell and the bending jig placed into the FE-SEM chamber for COD profile determination. Further details of the COD measurement are given in a previous report.[2]

The Raman spectroscopic apparatus (ISA, T 64000 Jovin-Yvon) was used for measuring the stresses as detected from fluorescence bands in Al_2O_3. An Ar-ion laser operating at a wavelength of 488 nm with a power of 300 mW was used as an excitation source, while an optical microscope was used both to focus the laser on the sample and to collect the scattered light. Frequencies of the scattered light were analyzed with a triple monochromator equipped with a charge-coupled device (CCD) camera. The dimension of the laser spot on the samples was 2 μm. Frequency shift due to the applied stress was monitored on the characteristic Gr^{3+} ruby lines $\mathbf{R}_1$, $\mathbf{R}_2$ of Al_2O_3 locate, at 14 400 and 14 430 cm^{-1}, respectively. The frequency used as the standard zero-value for the dense Al_2O_3/Al_2O_3-platelet body was recorded from the hot-pressed sample with a broad laser spot of several tens microns in absence of external stress.

The fluorescence spectra were analyzed with the curve-fitting algorithms included in the SpectraCalc software package (Galactic Industries Corp.). The bridging stresses were calculated from the measured frequency shift, according to the piezo-spectroscopic coefficients, Π_c and Π_a given in the literature as 2·75 and 2·10 cm^{-1} GPa^{-1} for an *a*- and *c*-axis oriented sapphire crystal, respectively.[12] Since it was not possible to distinguish the crystallographic orientation of each single Al_2O_3, grain under the optical microscope, the average piezo-spectroscopic coefficient, $\Pi_{av} = (\Pi_c + 2\Pi_a)/3$, was assumed to linearly relate the frequency shift to the nearly uniaxial bridging stress. Bridging stress data are also shown for comparison as collected on a toughened Si_3N_4

material. These latter data were obtained by using the shift of the 862 cm^{-1} Raman peak of Si_3N_4, while the experimental and computational procedures were the same as explained above for Al_2O_3. Further details of the Raman measurements in Si_3N_4 are reported in Ref. 2.

3 Results and Discussion

3.1 Bridging stress distribution

Determination of microscopic stresses from the shift of the ruby fluorescence lines was systematically performed along the entire crack-wake of several crack profiles. The cracks stably propagated for relatively large extensions (0·5–1 mm) in the Al_2O_3/Al_2O_3-platelet material. A crack was first propagated and arrested in the bending crack-stabilizer. Then, the specimen was dismounted front the crack-stabilizer and the loading jig placed into the fluorescence spectroscopy apparatus. Optical micrographs of the entire crack profile [shown in Fig. 1(a)] were taken *in-situ* upon reloading up to the nominal load value, P_c, critical for fracture. The crack profile is shown after its final failure in Fig. 1(b). Concurrently to optical observation, fluorescence spectra were recorded along the entire profile with a laser spot size of 2 μm. The distribution of stresses along the crack profile abscissa (at the loading condition $P \approx P_C$) is plotted in Fig. 2(a).

The first important feature of the stress profile is that all the stresses recorded at the loading condition $P \approx P_c$ were of a tensile nature. This means that they act as closure stresses on the crack face and, thus, they can be regarded as being bridging stresses. Another important characteristic of the stress distribution in Fig. 2(a) is that the magnitude of the bridging stresses was not uniform but showed a marked dependence on the abscissa, x′, along the crack profile. The function, σ_{BR} (x′), giving the bridging stress as a function of the crack-wake abscissa, x′, is an intrinsically discrete function because the stresses are generated at the individual bridging grains, as well as unbridged locations are also found along the crack profile. In the σ_{BR} (x′) function, a high stress region with a maximum of $\approx$350 MPa is noted in the initial 100 μm extension behind the crack tip. The remaining part of the profile, farther away from the crack tip, shows a statistically uniform distribution of stresses of minor magnitude $<$ 100 MPa.

In a previous *in-situ* Raman spectroscopy study,[2] the presence of a profile region with high bridging stress in the immediate neighborhood behind

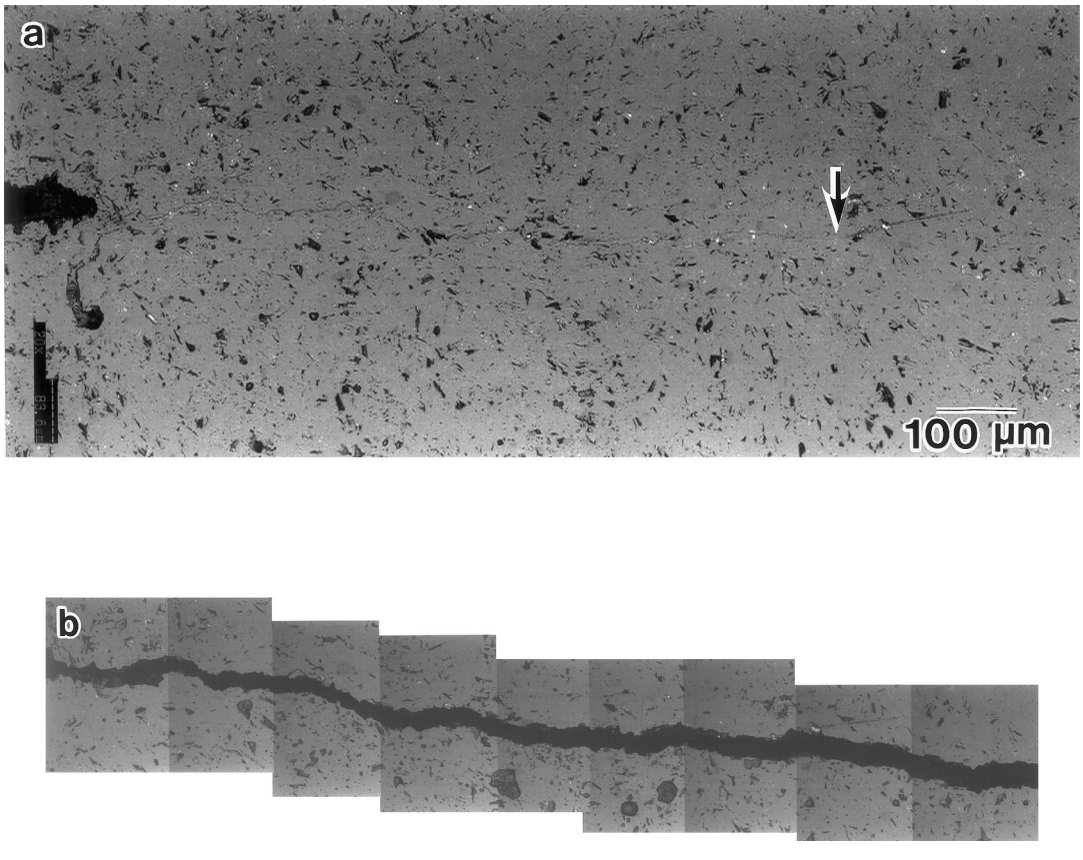

Fig. 1. Low magnification optical micrograph of a crack profile propagated from the notch tip in the Al_2O_3/Al_2O_3-platelet material. The micrograph in (a) is taken just before the occurrence of catastrophic fracture propagation (i.e. $P/P_c \approx 1$). In (b), the same zone of crack profile is shown after fracture. The large arrow locates the position of the crack tip.

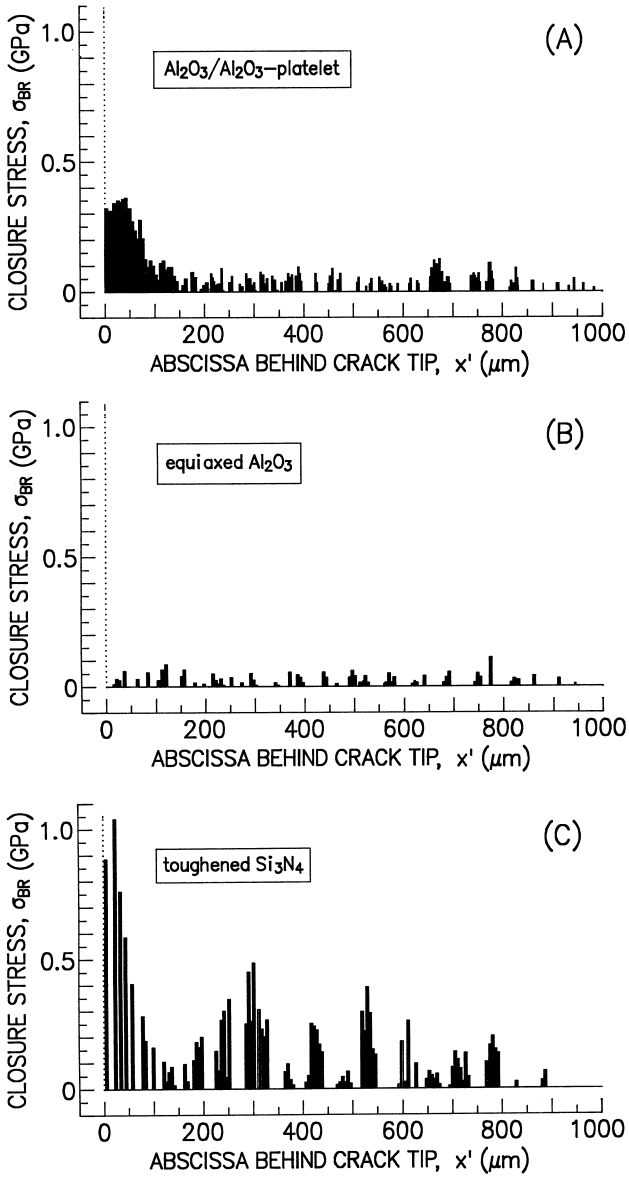

Fig. 2. (a) Map of local closure stresses as a function of the abscissa x' along the wake of the crack shown in Fig. 1. The map was performed with a laser spot of 2 μm, at $P/P_c \approx 1$. For comparison, maps collected in previous studies[1,2] and relative to similar crack extensions in a large-grained equiaxed Al_2O_3 and toughened Si_3N_4 are shown in (b) and (c), respectively.

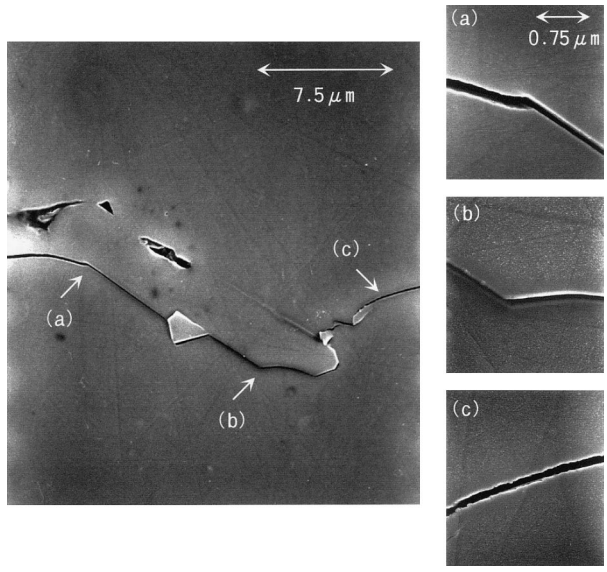

Fig. 3. FE–SEM micrograph showing a bridging site located in the immediate neighborhood behind a crack which stably propagated in the Al_2O_3/Al_2O_3-platelet specimen. Higher magnification images of the local COD profiles at the arrowed locations *a–c* are also shown for better clarity.

the crack tip has also been observed in a Si_3N_4 material toughened by (*in-situ* grown) acicular grains. On the other hand, equiaxed Al_2O_3, with average grain size similar to that of the present Al_2O_3 platelets, showed no region of high stress behind the tip. In equiaxed Al_2O_3, a discontinuous distribution of low magnitude bridging stresses (< 50 MPa) was found, almost independent of crack length.[1] The bridging stress distributions, found in previous studies[1,2] for both the equiaxed Al_2O_3 and the toughened Si_3N_4 are also shown for comparison in Fig. 2(b) and (c), respectively. The magnitude of bridging stress in the platelet-reinforced Al_2O_3 appears to be of an intermediate level between those of equiaxed Al_2O_3 and Si_3N_4 materials. In particular, the bridging stress found in the Al_2O_3/Al_2O_3-platelet material reaches only approximately one third of that of toughened Si_3N_4. The rationale for this difference in bridging stress magnitude is given in the next section, where the details of the microscopic fracture of the bridging sites are examined at higher magnification by SEM. The outcome of the present *in-situ* spectroscopy experiments is in agreement with the general notion that crystallites of elongated morphology promote the formation of a near-tip bridging zone in which high magnitude closure stresses can develop. In addition, *in-situ* spectroscopy provides a quantitative assessment of the bridging stress distribution. The average bridging stress over $\approx 800\,\mu$m crack profile was 68 MPa in Al_2O_3/Al_2O_3-platelet material against the 16 MPa found in equiaxed Al_2O_3 and the 148 MPa of toughened Si_3N_4.

3.2 Microscopic fracture processes and COD profile

Further information about the microscopic fracture process was obtained by SEM observation. A typical bridging site, observed in the zone of high bridging stress of the Al_2O_3/Al_2O_3-platelet material (cf. Fig. 2), is shown in Fig. 3. In this figure, higher magnification micrographs giving the details of the COD profile are also shown at various locations of the bridging site. The FE–SEM micrograph reveals that the interface surrounding the bridging platelet fractured in a large extent. In this case, pulling out should occur and frictional forces be generated at the sliding interfaces. However, due to the elongated morphology of the platelet and its inclination

with respect to the main crack plane, a marked interlocking effect is also developed upon increasing the COD until either complete pulling out or fracture of the platelet occurs.

The magnitude of closure stresses depends on precise microstructural characteristics, which will also dictate the morphology of the bridging zone. It has been generally recognized that the bridging effect can be either of elastic[13] or frictional[14] nature. Elastic bridging is obtained in polycrystalline ceramics when a grain/bridge is elastically pulled between the crack faces and finally fractures upon crack opening. Although partial interface debonding may initially occur, the interface of the bridging site does not completely fracture in the elastic bridging mechanism. The remarkable bridging stresses found in Si_3N_4 (cf. Fig. 2) arises from elastic bridging of acicular grains, although the extension of the bridging zone achievable in ceramics is rather limited.[15]

On the other hand, frictional bridging is the only source of toughening for ceramics with an equiaxed grain structure and weak interface strength. This bridging mechanism involves fracture of the interface at the bridging site before fracture strength of the individual bridging crystallites is reached. Although the frictional effect can occur over a large crack-wake extension, it does not usually allow for the development of bridging stresses of remarkable magnitude. This is the case of the equiaxed Al_2O_3 material[1] [cf. bridging stress distribution in Fig. 2(b)].

FE–SEM observation suggests that, although premature fracture of the interface in the present Al_2O_3/Al_2O_3-platelet material impedes the formation of elastic bridging sites, interlockings provide additional bridging tractions in the near-tip region. Interlocking sites are absent in equiaxed Al_2O_3, which is only affected by weak frictional effects. *In-situ* fluorescence spectroscopy shows that the characteristic magnitude of the bridging stress related to such interlocking effect is several hundreds MPa against the few tens MPa of frictional stresses.

Figure 4 shows the near-tip COD profile, which was measured by FE–SEM in the Al_2O_3/Al_2O_3-platelet composite. The profile presents a sigmoidal shape with the zone immediately behind the crack tip shielded for an extension of $\approx 100\,\mu$m. This crack extension well corresponds to the zone of higher bridging stress determined by fluoresence spectroscopy (cf. Fig. 2). This correspondence is regarded as a confirmation that the fluorescence spectroscopy approach can provide a physically sound estimate of the bridging distribution. It can be of interest to compare the COD profiles of the Al_2O_3/Al_2O_3-platelet composite with those of

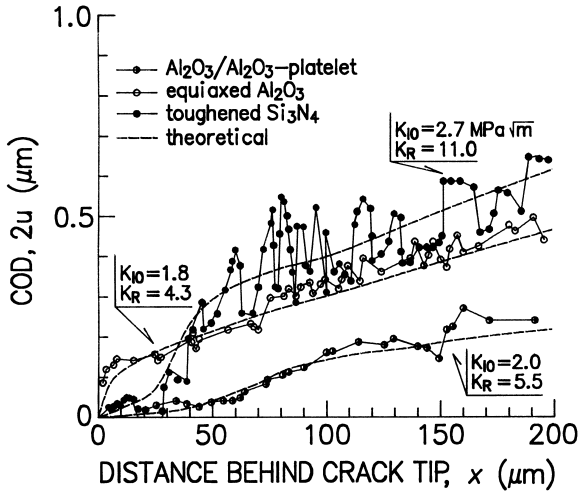

Fig. 4. Near-tip COD profile of an equilibrium crack in the Al_2O_3/Al_2O_3-platelet material. For comparison, COD profiles collected in previous studies[1,2] for equiaxed Al_2O_3 and toughened Si_3N_4 are also given. Experimental data are compared with theoretical predictions calculated according to eqns (2) and (3). Note the sigmoidal shape of the COD profile only found in those materials with high bridging stresses localized in the neighborhood behind the crack tip (cf. Fig. 2).

equiaxed Al_2O_3 and toughened Si_3N_4, as shown in Fig. 4. According to the presence of a zone of high bridging stress in the neighborhood of the crack tip, a sigmoidal COD profile can be found in Si_3N_4 and Al_2O_3/Al_2O_3-platelet. On the other hand, the profile of the equiaxed Al_2O_3 shows a nearly parabolic morphology, as expected in the case of a brittle crack free from any bridging traction.[16]

3.3 Macroscopic *R*-curve and microscopic fracture parameters

In Fig. 5, the rising *R*-curve behavior of the Al_2O_3/Al_2O_3-platelet material is shown, as determined by

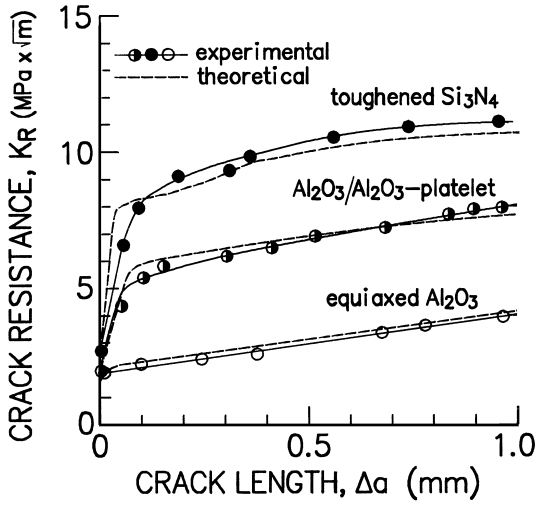

Fig. 5. The *R*-curve behavior of the Al_2O_3/Al_2O_3-platelet material as found by fracture mechanics measurements is compared with those of equiaxed Al_2O_3 and toughened Si_3N_4 from previous studies.[1,2] Theoretical curves are also shown as calculated [according to eqn (1)] from the distribution of the crack-wake closure stresses shown in Fig. 2.

fracture mechanics experiments upon a total crack extension $\Delta a \approx 1$ mm. The *R*-curve apparently starts rising from a critical stress intensity value, $K_{IO} \approx 2{\cdot}0\,MPa \times m^{1/2}$ up to a value $K_R \approx 8\,MPa \times m^{1/2}$ which is achieved after about 1 mm crack extension. The critical K_{IO} value for crack initiation, plotted at zero crack propagation in Fig. 5, was calculated using the nominal notch length and the load value at which the load-displacement curve deviated from linearity. For comparison, the rising *R*-curve behavior of toughened Si_3N_4 and equiaxed Al_2O_3 are also replotted in Fig. 5 from previous studies.[1,2] It is interesting to note that the sharp rising of crack resistance within the initial 100–200 μm crack extension is a characteristic only found in Al_2O_3/Al_2O_3-platelet and toughened Si_3N_4, namely, the materials whose near-tip zone shows high bridging stress (cf. Fig. 2). However, despite the similar K_{IO} values ($K_{IO} \approx 2{\cdot}0\,MPa \times m^{1/2}$ in Al_2O_3/Al_2O_3-platelet against the $2{\cdot}7\,MPa \times m^{1/2}$ of Si_3N_4) and a similar extension of near-tip bridging zone, the initial rising of crack resistance reaches in Si_3N_4 a 2 times higher value by virtue of the nearly three times higher magnitude of near-tip bridging stresses. It should also be noted from the *R*-curve behavior of the materials compared in Fig. 5 that frictional bridging stresses, although developed over a longer crack extension, can give only a minor contribution to the slope of rising *R*-curves.

The *R*-curve behavior experimentally determined by macroscopic fracture mechanics experiments can be compared with that theoretically calculated from the knowledge of the microscopic bridging stress distribution, σ_{BR} (x′), given in Fig. 2. If the bridging-stress distribution detected along a crack profile can be considered to be representative of that acting in the bulk, the rising *R*-curve component, ΔK, can be theoretically computed from the magnitude of the bridging tractions via the following equation:[16]

$$\Delta K = (2/\pi)^{1/2} \sum_{0}^{n}{}_{j} \int_{x_j}^{x_{j+1}} \sigma_{BR}\left(x'_j\right) \mathrm{d}x' / \sqrt{x'} \qquad (1)$$

where the index $j = 0, 1, 2, \ldots, n$ refers to the intervals of the discrete distribution of bridging stresses mapped by fluorescence or Raman spectroscopy. The variable x' locates the source point for the bridging stresses along the crack length, Δa, propagated from the notch root. Numerical integration of eqn (1) [using the bridging stress distributions $\Sigma_j \sigma_{BR}(x'_j)$ from Fig. 2] can be performed as a function of crack length, with assuming $0 < x' < \Delta a$, until covering the entire crack extension (i.e. ≈ 1 mm). This procedure allows the calculation of the rising *R*-curve behavior according to the equation, $K_R = K_{IO} + \Delta K$. The K_R results calculated from eqn (1) for the Al_2O_3/Al_2O_3-platelet material are shown in Fig. 5, in comparison with the toughened Si_3N_4 and the equiaxed Al_2O_3. As seen, the theoretical curves show (for all the materials) a good agreement with the experimental results. In particular, the steeply rising *R*-curves of materials with a high-stress near-tip bridging distribution can be predicted with good approximation, suggesting that the magnitude of bridging stresses determined *in-situ* by piezo-spectroscopy is basically correct.

In a previous paper,[2] a further proof that microprobe piezo-spectroscopic measurements can give a reasonable estimate of the magnitude of bridging stresses has been provided by using the COD profile. A similar approach is attempted here. The COD profile can be theoretically related to the bridging stress distribution, $\sigma_{BR}(x')$, according to the equation given by Barenblatt for a bridged equilibrium crack:[17]

$$u(x) = u_0(x) - (2/\pi E') \sum_{0}^{n}{}_{j} \int_{x_j}^{x_{j+1}} \sigma_{BR}\left(x'_j\right) \ln \left[\left| \left(\sqrt{x'} + \sqrt{x}\right) / \left(\sqrt{x'} - \sqrt{x}\right) \right| \right] \mathrm{d}x' \qquad (2)$$

where x is the abscissa along the COD profile with origin at the crack tip, E' is the plain strain Young's modulus (i.e. $E' = 453\ GPa$ in the present Al_2O_3/Al_2O_3-platelet material), and $\sigma_{BR}(x'_j)$ is the bridging stress function. $u_0(x)$, the term from which the shielding contribution by bridging stress has to be subtracted [cf. eqn (2)], is the theoretical COD profile which the crack would experience under a given applied K_R, if bridging stress are absent. It is given by the Irwin parabola:[16]

$$u_0(x) = [(K_R)/E'] \sqrt{(8x/\pi)} \qquad (3)$$

where K_R is the crack resistance experienced by the. material at the particular crack length under consideration. Introducing in eqn (2) the bridging stress distribution obtained by *in-situ* spectroscopy (Fig. 2) and the appropriate K_R value from the rising *R*-curve function, the COD profile can be theoretically predicted. The COD profile obtained from eqns (2) and (3) for the Al_2O_3/Al_2O_3-platelet material is shown by broken curve in Fig. 4, in comparison with the experimental data. As seen, the sigmoidal shape of the near-tip COD profile can be also predicted with good approximation by the Barenblatt equation, according to the bridging stress distribution of Fig. 2. This confirms that the near-tip COD morphology is directly related to the presence of a near-tip zone subjected to bridging

stresses of relatively high magnitude. This is the same characteristic which is also responsible for the sharply rising portion of the material *R*-curve. As a matter of fact, the COD profile of toughened Si_3N_4, which is also predictable from eqn (2)[2] (cf. Fig. 4), is markedly sigmoidal, while that of equiaxed Al_2O_3 is closer to the parabolic shape predicted by the Irwin eqn (3). The present COD data of equiaxed Al_2O_3 are in agreement with those recently reported by Seidel and Rödel[18] for a monolithic Al_2O_3 material with a similar grain size. The good agreement between theoretical and experimental COD profiles may strengthen the main notion given in this paper that the magnitude of bridging stresses can be reasonably addressed by *in-situ* piezo-spectroscopy.

4 Conclusions

In-situ fluorescence microprobe spectroscopy has been applied to measure the bridging stress distribution developed in the crack-wake during stable fracture in Al_2O_3/Al_2O_3-platelet ceramic. These experiments, coupled with FE-SEM observation, have provided the rationale on the microscopic scale for the toughening effect (i.e. rising *R*-curve behavior) found by macroscopic fracture experiments. Although the rather weak intergranular bond of polycrystalline Al_2O_3 does not allow for any elastic bridging site to develop (as for example found in toughened Si_3N_4 materials) a marked interlocking effect can be provided upon crack opening in presence of high-aspect-ratio platelets. A near-tip zone of bridging stresses with relatively high magnitude was found in a crack-wake zone $< 100\,\mu$m behind the crack tip. At the K_R value required for crack extension, these near-tip bridging sites supported a maximum tensile stresses of ≈ 350 MPa. Of lower magnitude were the stresses measured in correspondence of frictional sites farther away from the crack tip.

The bridging stress distribution determined by microprobe fluorescence spectroscopy was used to theoretically predict the rising *R*-curve behavior of the Al_2O_3/Al_2O_3-platelet material. A comparison between theoretical and experimental *R*-curve data showed a satisfactory agreement, confirming that the bridging stress distribution collected by fluorescence spectroscopy are reliable and proving that crack bridging can be invoked as the main toughening mechanism in the present Al_2O_3/Al_2O_3 material.

A further proof of the consistency of microscopic and macroscopic fracture data has been provided by monitoring the morphology of the near-tip COD profile. A near-tip COD profile sigmoidal rather than parabolic, reflected the presence of relevant bridging stresses in the very neighborhood behind the crack tip. The near-tip sigmoidal shape of the COD profile, which is a peculiarity of highly tough ceramics, could be reasonably explained according to a theoretical computation using the bridging stress distribution experimentally determined by microprobe fluorescence spectroscopy.

Acknowledgements

The authors sincerely thank Toray Research Center for the use of the Raman spectroscope. Discussions with Professor J. Rödel and Dr M. Hoffman are also sincerely acknowledged. This work has been supported by the Toray Foundation.

References

1. Pezzotti, G., Sbaizero, O., Sergo, V., Muraki, N., Maruyama, K. and Nishida, T., *In-situ* measurements of frictional bridging stresses in alumina using fluorescence spectroscopy. *J. Am. Ceram. Soc.*, 1998, **81**, 187–192.
2. Pezzotti, G., Muraki, N., Maeda, N., Satou, K. and Nishida, T. *In-situ* measurement of bridging stresses in toughened Si_3N_4 using Raman microprobe spectroscopy. *J. Am. Ceram. Soc.*, in press.
3. Pezzotti, G., Suenobu, H., Nishida, T. and Sbaizero, O. Measurement of microscopic bridging stresses in alumina/molybdenum composite by *in-situ* fluorescence spectroscopy. *J. Am. Ceram. Soc.*, in press.
4. Pezzotti, G., Muraki, N. and Nishida, T. Microprobe piezo-spectroscopy for the micromechanical analysis of fracture and deformation phenomena in polycrystalline ceramics. *Composite Sci. and Tech.*, in press.
5. Pezzotti, G., Sbaizero, O. and Nishida, T. Basic study of fracture mechanisms in polycrystalline ceramics using *in-situ* fluorescence and Raman microprobe spectroscopy. *Proceedings of CIMTEC '98*, in press.
6. Becher, P. F., Hwang, S.-L. and Hsueh, C.-H., Using microstructure to attack the brittle nature of silicon nitride ceramics. *MRS Bull.*, 1995, **10**, 23–27.
7. Mai, Y.-W. and Lawn, B. R., Crack-interface grain bridging as a fracture resistance mechanism in ceramics: II, theoretical fracture mechanics model. *J. Am. Ceram. Soc.*, 1987, **70**, 289–294.
8. Rödel, J., Kelly, J. F. and Lawn, B. R., *In-situ* measurements of bridged crack interfaces in the scanning electron microscope. *J. Am. Ceram. Soc.*, 1990, **73**, 3313–3318.
9. Nishida, T., Hanaki, Y. and Pezzotti, G., Effect of notch-root radius on the fracture toughness of a fine-grained alumina. *J. Am. Ceram. Soc.*, 1995, **77**, 606–608.
10. Nojima, T. and Nakai, O., Stable crack extension of an alumina ceramic in three-point bending test. *J. Soc. Mater. Sci. Jpn.*, 1993, **42**, 412–418 (in Japanese).
11. Nishida, T., Hanaki, Y., Nojima, T. and Pezzotti, G., Measurement of rising *R*-curve behavior in toughened silicon nitride by stable crack propagation in bending. *J. Am. Ceram. Soc.*, 1995, **78**, 3113–3116.
12. He, J. and Clarke, D. R., Determination of the piezospectroscopic coefficients for chromium-doped sapphire. *J. Am. Ceram. Soc.*, 1995, **78**, 1347–1353.
13. Hsueh, C. H. and Becher, P. F., Evaluation of bridging stress for *R*-curve behavior of nontransforming ceramics. *J. Am. Ceram. Soc.*, 1988, **71**, C–234-237.

14. Swanson, P. L., Fairbanks, C. J., Lawn, B. R., Mai, Y.-W. and Hockey, B. J., Crack-interface grain bridging as a fracture resistance mechanism in ceramics: I, experimental study on alumina. *J. Am. Ceram. Soc.*, 1987, **70**, 279–289.
15. Pezzotti, G., Okamoto, Y., Nishida, T. and Sakai, M., On the near-tip toughening by crack-face bridging in particulate and platelet-reinforced ceramics. *Acta Mater.*, 1996, **44**, 899–914.
16. Irwin, G. R., Fracture. In *Handbuch der Physik*, Vol. 6. Springer–Verlag. Berlin, 1958, pp. 551–594.
17. Barenblatt, G. I., The mathematical theory of equilibrium cracks in brittle fracture. *Adv. Appl. Mech.*, 1962, **7**, 55–129.
18. Seidel, J. and Rödel, J., Measurement of crack tip toughness in alumina as a function of grain size. *J. Am. Ceram. Soc.*, 1997, **80**, 433–438.